A Finite Input Alphabet Perspective on the Rate-Energy Tradeoff in SWIPT over Parallel Gaussian Channels

Rakshith Rajashekar, *Senior Member, IEEE*, Marco Di Renzo, *Senior Member, IEEE*, Lie-Liang Yang, *Fellow, IEEE*, K.V.S. Hari, *Fellow, IEEE*, and L. Hanzo, *Fellow, IEEE*

***Abstract*—Simultaneous wireless information and power transfer (SWIPT) has gained significant popularity in the recent past owing to its applications in a wide range of use-cases. Although SWIPT has been fairly well investigated in the literature, the existing work has mainly focused on attaining the optimal rate energy (RE) trade-off assuming Gaussian input alphabet. However, practical systems operate with finite input alphabets such as QAM/PSK. We characterise the attainable RE trade-off in SWIPT systems employing finite input alphabet for transmission over parallel Gaussian channels of say orthogonal frequency division multiplexing subcarriers or multiple-input multiple-output streams. Some of the key results in the literature that assume Gaussian input alphabet are shown to be special cases of our results. Furthermore, we provide insights into our results with the aid of graphical illustrations, which throw light on the optimal power allocation policy for various energy harvesting constraints. Furthermore, we consider practically relevant time sharing and power splitting schemes operating with finite input alphabet and characterise their RE trade-off. Their optimal solutions in the asymptotic regime are obtained, which serve as low-complexity solutions suitable for practical implementation. Our simulation studies have demonstrated that the Gaussian input assumption significantly over-estimates the attainable RE trade-off, especially when the signal set employed is small. Furthermore, it is observed through numerical simulations that the proposed optimal power allocation performs significantly better than the power allocation based on the Gaussian input assumption. Specifically, as much as 30% rate improvement is observed when employing the classic 4-QAM signal set.**

***Index Terms*—Rate-energy trade-off, SWIPT, parallel Gaussian channels, finite input constellations, time sharing and power splitting.**

R. Rajashekar, L.-L. Yang and L. Hanzo are with the School of ECS, University of Southampton, Southampton SO17 1BJ, UK (e-mail: rmr1u14@soton.ac.uk, lly@ecs.soton.ac.uk, lh@ecs.soton.ac.uk).

M. Di Renzo is with the Laboratoire des Signaux et Systemes, CNRS, Centrale Supelec, Univ Paris Sud, Universite Paris-Saclay, 3 rue Joliot Curie, Plateau du Moulon, 91192, Gif-sur-Yvette, France. (e-mail: marco.direnzo@l2s.centralesupelec.fr). His work is partially supported by the European Commission (EC) through the H2020-ETN-5Gwireless research project (grant 641985) and by the Agence Nationale de la Recherche Scientifique (ANR) through the SpatialModulation research project (Societe de l'Information et de la Communication - Action Plan 2015.

K.V.S. Hari is with the Dept. of ECE, Indian Institute of Science, Bangalore - 560012, India (e-mail: hari@iisc.ac.in).

The financial support of the EPSRC projects EP/P034284/1, EP/N004558/1 and EP/L018659/1, as well as of the ERC's Advanced Fellow Award QuantCom is gratefully acknowledged. All data supporting this study are openly available from the University of Southampton repository at https://doi.org/10.5258/SOTON/D0627.

I. Introduction

The number of networked devices is expected to proliferate owing to a wide range of compelling applications [1], such as smart sensors in home applications, wearable devices, environmental sensors, warehouse management etc. Since most of these devices are battery operated, it is imperative that they have high energy-efficiency. While harvesting energy from the environment is well investigated, the recently emerged simultaneous wireless information and power transfer (SWIPT) philosophy [2]-[4] has gained significant popularity owing to its capability of extending the lifespan of the battery-operated devices. SWIPT was first proposed in [5] and its various extensions were studied in [6]-[11]. Specifically, Grover and Sahai studied the SWIPT in frequency-selective additive white Gaussian noise (AWGN) channels [6]. Zhang and Ho characterised the rate-energy (RE) trade-off in multiple-input multiple-output (MIMO) SWIPT systems operating relying both on co-located as well as spatially separated energy harvesting (EH) and information decoding (ID) receivers [7]. Furthermore, Zhou *et al.* proposed dynamic power splitting aided SWIPT and characterised its RE trade-off [8]. They also studied the performance of SWIPT in the downlink of multiuser communication by considering both time sharing (TS) and power splitting (PS) receivers [9]. A detailed overview of various existing SWIPT schemes as well as the challenges and open issues of practical SWIPT systems can be found in [10], [11].

A key requirement of SWIPT systems is that they require channel state information (CSI) at the transmitter for energy/information beamforming. Hence, several beamforming schemes have been proposed for SWIPT systems [12]-[16], which focus on reducing the CSI feedback overhead while maximizing both the energy as well as the information efficiencies. Specifically, adaptive energy beamforming was proposed in [12] in conjunction with a CSI quantization scheme for improving the power vs. information transmission trade-off. In [13], Shi *et al.* studied the joint optimization of the transmit beamforming and the receive power splitting in a multiuser downlink communication scenario. As a further development, Park and Clerckx focused on reducing the CSI feedback overhead in MIMO interference channel with the aid of Geodesic energy beamforming [14], which requires partial CSI. Low-cost alternatives such as antenna selection and hybrid beamforming aided SWIPT schemes were investigated by

Demir and Tuncer [15]. Recently, SWIPT was also studied by Yang *et al.* in the context of millimeter wave communication by considering lens antenna arrays [16].

However, the existing SWIPT solutions discussed so far were conceived by considering Gaussian input alphabet, which do not model the practical communication systems, where finite signal sets such as QAM/PSK are employed. It is widely recognized that when using a finite input alphabet, the achievable performance of transmission schemes under the Gaussian input assumption is significantly lower than that of the finite input alphabet. This phenomenon has been extensively studied both in scalar as well as vector Gaussian channels [17], [18] relying on transmit power allocation/precoding schemes [19]-[23]. Recently, the performance degradation due to Gaussian input assumption in SWIPT systems operating with finite input alphabet has been studied in [24]-[26]. Specifically, Zewde and Gursoy [24] have studied the RE trade-off in a point-to-point SWIPT system by optimizing the probabilities associated with the input constellation points. Furthermore, the authors of [25], [26] have characterised the RE trade-off in precoded MIMO systems employing finite input alphabet. Although [24]-[26] provide some insights, the implications of having finite input alphabets on the RE trade-off remain largely unexplored.

Against this background, the following are the contributions of this paper:

1) Orthogonal frequency division multiplexing (OFDM) [27], MIMO systems employing singular value decomposition (SVD) aided beamforming [28], etc. are some of the well-known scenarios of parallel Gaussian channels, whose RE trade-off remains unknown in case of finite input alphabet. In this paper, we first characterise the RE trade-off of SWIPT systems operating with finite input alphabet over parallel Gaussian channels, and show that the seminal results on co-located EH and ID receivers presented in [7] are special cases of our results. Furthermore, we provide insights into our results with the aid of graphical illustrations and show them to be a generalization of the well-known *mercury-water pouring* algorithm [19].
2) We consider practically relevant TS as well as PS schemes and characterise their RE trade-off by considering finite input alphabets. Furthermore, we obtain asymptotic high signal-to-noise ratio (SNR) results on power allocation for these schemes, and compare them to their non-asymptotic counterparts. Since the SWIPT systems have to operate at high SNR for gleaning sufficient energy, our asymptotic high-SNR results are shown to be a simple solution for the practical implementation of the aforementioned schemes. Furthermore, we quantify the suboptimality of the Gaussian input assumption in terms of the attainable mutual information (MI) and harvested energy, and show how substantial it is when the signal set employed is small.

For the ease of reading, the paper provides tutorial insights interspersed with analytical and numerical results. The organization of the paper is as follows. The system model as well as the definitions and terminologies used in the paper are presented in Section II. Our main results on the RE trade-off in SWIPT systems operating with finite input alphabet are presented in Section III. The graphical illustrations of our results are presented in Section IV. The TS and PS schemes are discussed in the context of finite input alphabet and their asymptotic behaviours are studied in Section V. Our conclusions are presented in Section VI.

Notations: $\mathbb{R}$ and $\mathbb{C}$ represent the field of real and complex numbers, respectively. The notation of $|\cdot|$ represents the magnitude of a complex quantity, or the cardinality of a given set. Expected value of a random variable z is denoted by $\mathbb{E}[z]$. Given a random variable y, $\mathbb{E}[z|y]$ represents the conditional mean of z given y. A complex-valued circularly symmetric Gaussian distribution with a mean of μ and a variance of σ^2 is denoted by $\mathcal{CN}(\mu, \sigma^2)$. The maximization problem is denoted by $\mathtt{max}_{v_1,\cdots,v_N}$, where $v_1, \ldots, v_N$ are the optimization variables. The mutual information is measured in nats/channel use, unless stated otherwise.

II. System Model

Consider a single-user SWIPT system consisting of a transmitter and a receiver having co-located EH and ID blocks. Both the energy as well as the information are transmitted to the receiver over N parallel channels. Explicitly, the N channels may correspond to the N orthogonal subcarriers in case of an OFDM system, or N parallel data streams in case of an $N \times N$ MIMO system employing beamforming [28]. We consider a generic system model so that the results derived can be readily applied to various scenarios. Let the N parallel Gaussian channels be modeled as

$$y_i = h_i x_i + n_i, \qquad i = 1, 2, \ldots, N, \tag{1}$$

where $y_i \in \mathbb{C}$ is the signal received over the i^{th} channel, $h_i \in \mathbb{C}$ is the i^{th} channel coefficient, $n_i \sim \mathcal{CN}(0,1)\ \forall\ i$, and x_i is the symbol transmitted over the i^{th} channel. The transmitted symbol x_i satisfies the power constraint

$$\frac{1}{N}\sum_{i=1}^{N} \mathbb{E}\left[|x_i|^2\right] \leq P, \tag{2}$$

and it is modeled as $x_i = \sqrt{p_i P} s_i$, where p_i is the power allocation factor, which satisfies

$$\sum_{i=1}^{N} p_i \leq N, \tag{3}$$

and s_i is the equiprobable information bearing symbol chosen from a unit-energy constellation $\mathcal{S}_i$.

The SNR over the i^{th} channel is represented by $\rho_i = p_i \gamma_i$, where $\gamma_i = |h_i|^2 P$. Without loss of generality, we assume $\gamma_1 \geq \gamma_2 \geq \cdots \geq \gamma_N$.

Definition 1: The total achievable MI over the N parallel channels for a given power allocation $\{p_1, \ldots, p_N\}$ is given by

$$R = \mathcal{I}(\rho_1, \rho_2, \ldots, \rho_N) = \sum_{i=1}^{N} \mathcal{I}_i(\rho_i), \tag{4}$$

where the achievable MI over the i^{th} channel at an SNR ρ_i is given by

$$\mathcal{I}_i(\rho_i) = \mathcal{I}_i(s_i; \sqrt{\rho_i}s_i + n_i), \tag{5}$$

$$= \log M_i - \frac{1}{M_i}\sum_{s\in\mathcal{S}_i}\mathbb{E}\left[\log\left\{\sum_{s'\in\mathcal{S}_i}\exp\left(\Psi_{s,s'}\right)\right\}\right], \tag{6}$$

where $M_i = |\mathcal{S}_i|$ and $\Psi_{s,s'} = -|\sqrt{\rho_i}(s-s') + n_i|^2 + |n_i|^2$.

Definition 2: The total power received over the N parallel channels is given by

$$\bar{Q} = \eta\sum_{i=1}^{N}\mathbb{E}\left[|h_i x_i|^2\right], \tag{7}$$

$$= \eta\sum_{i=1}^{N} p_i\gamma_i, \tag{8}$$

where η denotes the energy harvesting efficiency [7], which is taken to be one for the ease of presentation.

Definition 3: The minimum mean-squared error (MMSE) in the estimation of the i^{th} symbol s_i at an SNR ρ_i is given by

$$\texttt{MMSE}_i(\rho_i) = \mathbb{E}\left[|s_i - \hat{s}_i(y_i,\rho_i)|^2\right], \tag{9}$$

where

$$\hat{s}_i(y_i,\rho_i) = \mathbb{E}\left[s_i | y_i = \sqrt{\rho_i}s_i + n_i\right], \tag{10}$$

$$= \frac{\sum_{s\in\mathcal{S}_i} s e^{-|y_i - \sqrt{\rho_i}s|^2}}{\sum_{s\in\mathcal{S}_i} e^{-|y_i-\sqrt{\rho_i}s|^2}}. \tag{11}$$

Closed-form expressions of $\texttt{MMSE}_i(\rho_i)$ for various signal sets such as BPSK, QPSK, 16-QAM etc. can be found in [19]. Furthermore, the inverse function of $\texttt{MMSE}_i(\rho_i)$, which is required in our subsequent analysis for various signal sets, can be stored in a look-up table.

The following proposition proves instrumental in characterising the RE trade-off in Section III.

Proposition 1: [17] The MI and the MMSE associated with the i^{th} channel satisfy

$$\frac{d}{d\rho_i}\mathcal{I}_i(\rho_i) = \texttt{MMSE}_i(\rho_i). \tag{12}$$

III. RE Tradeoff in SWIPT Systems Operating with Finite Input Alphabet

In order to characterise the RE trade-off, we first consider the two extreme cases, where only either the EH receiver or the ID receiver is present, followed by the case where both the EH and ID receivers operate concurrently. Considering only the EH receiver to be present, the objective is to maximize the harvested energy $\bar{Q} = \sum_{i=1}^{N} p_i\gamma_i$. Thus, we have the following optimization problem:

$$\text{P1:} \quad \max_{\{p_1,\ldots,p_N\}} \quad \bar{Q} = \sum_{i=1}^{N} p_i\gamma_i$$
$$\texttt{s.t.} \quad \sum_{i=1}^{N} p_i \le N,\ p_i \ge 0\ \forall\ i.$$

Proposition 2: The solution to (P1) is given by $p_1 = N$ and $p_j = 0$ for $2 \le j \le N$.

Proof: The proof directly follows from the fact that $\gamma_1 \ge \gamma_j$ for $2 \le j \le N$, which is essentially the popular energy beamforming solution [10]. ■

The maximum harvested energy in this case is given by $\bar{Q}_{max} = N\gamma_1$. If the ID receiver were to operate concurrently with the EH receiver, the attainable MI is given by $R_{EH} = \mathcal{I}_1(N\gamma_1) \le \log(M_1)$. If the system were to operate with the idealized Gaussian input alphabet, we have $R_{EH} = \log(1+N\gamma_1) = \log(1+N|h_1|^2P)$, which grows unbounded with P. By contrast, in the practical finite input alphabet case R_{EH} is upperbounded by $\log(M_1)$. This key difference plays an important role in optimally exploiting the available power for striking the most appropriate information vs. energy transmission trade-off as discussed in the subsequent sections.

Assuming only the ID receiver to be present, the objective is to maximize the attainable rate $R = \sum_{i=1}^{N}\mathcal{I}_i(p_i\gamma_i)$. Thus, we have the following optimization problem:

$$\text{P2:} \quad \max_{\{p_1,\ldots,p_N\}} \quad \sum_{i=1}^{N}\mathcal{I}_i(p_i\gamma_i)$$
$$\texttt{s.t.} \quad \sum_{i=1}^{N} p_i \le N,\ p_i \ge 0\ \forall\ i.$$

Proposition 3: The solution to (P2) is given by the well-known mercury-water pouring algorithm [19]:

$$p_i^{\texttt{MWP}} = \frac{1}{\gamma_i}\texttt{MMSE}_i^{-1}\left(\min\left\{1, \frac{\mu}{\gamma_i}\right\}\right), \quad i = 1,\ldots,N, \tag{13}$$

where μ is the solution to

$$\sum_{\substack{i=1\\ \mu<\gamma_i}}^{N}\frac{1}{\gamma_i}\texttt{MMSE}_i^{-1}\left(\frac{\mu}{\gamma_i}\right) = N. \tag{14}$$

The maximum attainable MI in this case is given by $R_{max} = \sum_{i=1}^{N}\mathcal{I}_i(p_i^{\texttt{MWP}}\gamma_i)$. If the EH receiver was to operate concurrently with the ID receiver, the attainable energy transmission would be given by $\bar{Q}_{ID} = \sum_{i=1}^{N} p_i^{\texttt{MWP}}\gamma_i$. Thus, the two extremities of the RE region are given by $(R_{EH}, \bar{Q}_{max})$ and $(R_{max}, \bar{Q}_{ID})$. Note that while attaining $\bar{Q}_{max}$, any rate obeying $R < R_{EH}$ can be achieved by reducing the coding rate employed by the transmitter.

In order to characterize all the legitimate RE pairs in the region

$$\mathcal{E}(P) \triangleq \Big\{(R,\bar{Q}) : R \le \sum_{i=1}^{N}\mathcal{I}_i(p_i\gamma_i), \bar{Q} \le \sum_{i=1}^{N} p_i\gamma_i, \sum_{i=1}^{N} p_i \le N, p_i \ge 0\ \forall\ i\Big\}, \tag{15}$$

we now consider $R_{EH} < R < R_{max}$ and $\bar{Q}_{ID} < \bar{Q} < \bar{Q}_{max}$, which leads us to the following optimization problem:

$$\text{P3:} \quad \max_{\{p_1,\ldots,p_N\}} \quad \sum_{i=1}^{N} \mathcal{I}_i(p_i\gamma_i)$$
$$\texttt{s.t.} \quad \sum_{i=1}^{N} p_i\gamma_i \geq \bar{Q}, \sum_{i=1}^{N} p_i \leq N,\ p_i \geq 0\ \forall\ i.$$

Proposition 4: The solution to (P3) is given by

$$p_i^{\texttt{MGP}} = \begin{cases} \frac{1}{\gamma_i}\texttt{MMSE}_i^{-1}\left(\frac{\mu-\lambda\gamma_i}{\gamma_i}\right), & \text{if } \mu < (1+\lambda)\gamma_i \\ 0, & \text{otherwise} \end{cases} \tag{16}$$

for $i = 1, \ldots, N$, where μ and λ are solutions to

$$\sum_{\substack{i=1 \\ \mu<(1+\lambda)\gamma_i}}^{N} \frac{1}{\gamma_i}\texttt{MMSE}_i^{-1}\left(\frac{\mu-\lambda\gamma_i}{\gamma_i}\right) = N, \tag{17}$$

and $\mu > \lambda\gamma_1$. The power allocation in (16) is referred to as the *mercury-gallium pouring*[1] algorithm.

Proof: The objective function in (P3) is concave over the constraint set, since each of the MI functions is strictly concave over its input power. The Lagrangian [29] of (P3) is given by

$$\mathcal{L}(\{p_1,\ldots,p_N\},\lambda,\mu) = \sum_{i=1}^{N}\mathcal{I}_i(p_i\gamma_i) + \lambda\left(\sum_{i=1}^{N} p_i\gamma_i - \bar{Q}\right) + \mu\left(N - \sum_{i=1}^{N} p_i\right), \tag{18}$$

and the Lagrange dual function of (P3) is given by

$$\mathcal{G}(\lambda,\mu) = \max_{\{p_1,\ldots,p_N\}} \mathcal{L}(\{p_1,\ldots,p_N\},\lambda,\mu). \tag{19}$$

Since the solution to (P3) can be obtained by solving $\min_{\mu\geq 0,\lambda\geq 0}\mathcal{G}(\lambda,\mu)$, we first solve the problem in (19) for a fixed λ and μ. We have

$$\mathcal{G}(\lambda,\mu) \triangleq \max_{\{p_1,\ldots,p_N\}} \sum_{i=1}^{N}\mathcal{I}_i(p_i\gamma_i) - (\mu-\lambda\gamma_i)p_i, \tag{20}$$

and the first-order necessary conditions for optimality [29] are given by

$$\frac{d}{dp_i}\mathcal{I}_i(p_i\gamma_i) - (\mu-\lambda\gamma_i) = 0, \tag{21}$$
$$\lambda\left(\sum_{i=1}^{N} p_i\gamma_i - \bar{Q}\right) = 0, \tag{22}$$
$$\mu\left(N - \sum_{i=1}^{N} p_i\right) = 0, \tag{23}$$
$$\mu \geq 0, \tag{24}$$
$$\lambda \geq 0. \tag{25}$$

[1]Note that the density of Gallium is 5.91 g/cm^3, which is much lighter than mercury whose density is 13.69 g/cm^3. The choice of Gallium is to highlight the fact that the solution to (P3) would not have a constant *water-level* as in the case of the mercury-water pouring algorithm [19].

It is readily inferred from (20) that it is necessary to have $\mu > \lambda\gamma_1$ in order to have a bounded solution. From Proposition 1, we have

$$\frac{d}{dp_i}\mathcal{I}_i(p_i\gamma_i) = \gamma_i\texttt{MMSE}_i(p_i\gamma_i), \tag{26}$$

and hence the optimal power allocation should satisfy

$$\gamma_i\texttt{MMSE}_i(p_i\gamma_i) = \mu - \lambda\gamma_i, \tag{27}$$
$$\implies p_i^{\texttt{MGP}} = \frac{1}{\gamma_i}\texttt{MMSE}_i^{-1}\left(\frac{\mu-\lambda\gamma_i}{\gamma_i}\right). \tag{28}$$

Since the domain of $\texttt{MMSE}_i^{-1}(\cdot)$ is $[0,1]$, we have the condition $\mu < (1+\lambda)\gamma_i$ for $i = 1,\ldots,N$. The optimal μ and λ for a given set of $\{p_1,\ldots,p_N\}$ can be obtained by employing the well-known subgradient techniques [29]. The solution to (P3) can be obtained by iterating between the primal and dual solutions until convergence. Specifically, for a given $\mu \geq 0$, $\lambda \geq 0$ the sub-gradient of the dual metric is computed: $\left[\sum_{i=1}^{N} p_i\gamma_i - \bar{Q},\ N - \sum_{i=1}^{N} p_i\right]$, which is used for updating (μ,λ) based on the ellipsoid method. From the new set of (μ,λ), p_i is updated based on (27). This procedure is repeated until μ and λ converge to a prescribed accuracy. This concludes the proof. ■

The following corollary provides the optimal power allocation for the Gaussian input assumption, which was studied in [7].

Corollary 1: When each of the inputs obeys $s_i \sim \mathcal{CN}(0,1)$, then the optimal power allocation in (16) reduces to

$$p_i = \begin{cases} \frac{1}{\mu-\lambda\gamma_i} - \frac{1}{\gamma_i}, & \text{if } \mu < (1+\lambda)\gamma_i \\ 0, & \text{otherwise} \end{cases} \tag{29}$$

for $i = 1,\ldots,N$.

Proof: When $s_i \sim \mathcal{CN}(0,1)$, we have $\mathcal{I}_i(p_i\gamma_i) = \log(1+p_i\gamma_i)$ for $i = 1,\ldots,N$ and from Proposition 1, we have

$$\frac{d}{dp_i}\mathcal{I}_i(p_i\gamma_i) = \frac{\gamma_i}{1+p_i\gamma_i}. \tag{30}$$

From (21), we have $\frac{\gamma_i}{1+p_i\gamma_i} = (\mu-\lambda\gamma_i) \implies 1 + p_i\gamma_i = \frac{\gamma_i}{\mu-\lambda\gamma_i} \implies p_i = \left(\frac{1}{\mu-\lambda\gamma_i} - \frac{1}{\gamma_i}\right)$. This concludes the proof. ■

Let us now compare the attainable RE trade-off in a SWIPT system employing either Gaussian or finite input alphabets. Fig. 1 compares the RE trade-off attained by various constellations in a SWIPT system having $N = 2$, $\gamma_1 = 4$ and $\gamma_2 = 1.2$. It is evident from Fig. 1 that the Gaussian input assumption results in a significant over-estimation of the RE trade-off, especially when the constellation employed is small. Furthermore, it can be seen from Fig. 1 that the discrepancy between the pair of trade-offs reduces, as the constellation size is increased. This is expected, since a high-order constellation is a better approximation of the Gaussian input.

So far, we considered co-located EH and ID receivers, which is practically more relevant than the case, where the pair of receivers are separated. Nonetheless, our results can be readily extended to the case of spatially separated receivers as well, which is briefly discussed below.

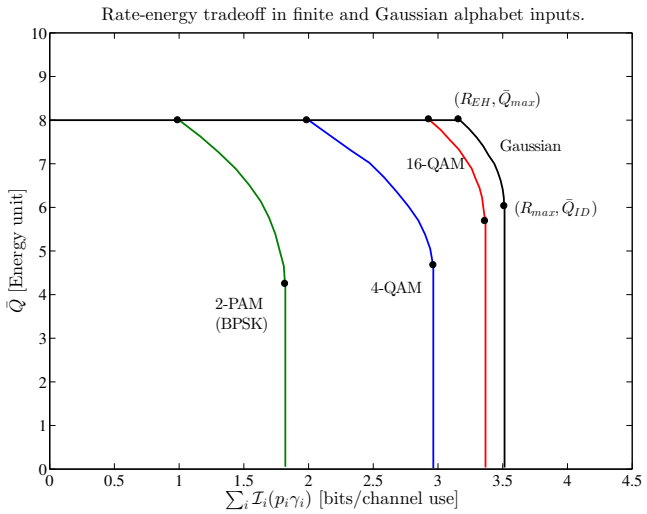

Fig. 1. Comparison of the RE trade-off in Gaussian and finite input alphabets in a SWIPT system having $N = 2$, $\gamma_1 = 4$ and $\gamma_2 = 1.2$.

Let $\{\gamma_i\}_{i=1}^N$ and $\{\gamma_i'\}_{i=1}^N$ represent the set of channel gains over the N parallel channels spanning from the transmitter to the ID and EH receivers, respectively. Furthermore, let $\gamma'_{max} = \max_i \gamma_i'$ and $i'_{max} = \arg\max_i \gamma_i'$. Proceeding along the lines of Proposition 3 and Proposition 4, we have $R_{max} = \sum_{i=1}^N \mathcal{I}_i(p_i^{\texttt{MWP}}\gamma_i)$, $\bar{Q}_{ID} = \sum_{i=1}^N p_i^{\texttt{MWP}}\gamma_i'$, $R_{EH} = \mathcal{I}_{i'_{max}}(p_{i'_{max}}^{\texttt{MWP}}\gamma_{i'_{max}})$ and $\bar{Q}_{max} = N\gamma'_{max}$. The optimal power allocation for the case of spatially separated EH and ID receivers is given by the following proposition.

Proposition 5: The optimal power allocation for the case of separated EH and ID receivers is given by

$$p_i^{\texttt{MGP}} = \begin{cases} \frac{1}{\gamma_i}\texttt{MMSE}_i^{-1}\left(\frac{\mu-\lambda\gamma_i'}{\gamma_i}\right), & \text{if } \mu < \gamma_i + \lambda\gamma_i' \\ 0, & \text{otherwise} \end{cases} \tag{31}$$

for $i = 1, \ldots, N$, where μ and λ are solutions to

$$\sum_{\substack{i=1 \\ \mu<\gamma_i+\lambda\gamma_i'}}^{N} \frac{1}{\gamma_i}\texttt{MMSE}_i^{-1}\left(\frac{\mu-\lambda\gamma_i'}{\gamma_i}\right) = N, \tag{32}$$

and $\mu > \lambda\gamma'_{max}$.
The proof is similar to that of Proposition 4, hence it is omitted due to space constraints. Note that since EH receivers are not capable of sophisticated signal processing, the channel gains $\{\gamma_i'\}_{i=1}^N$ may not be made available to the transmitter for employing the optimal power allocation presented in Proposition 5. In this paper, we focus only on SWIPT systems having co-located EH and ID receivers.

IV. Graphical Illustrations

In this section, we provide further insights into the solution of (P3) presented in Section III with the aid of graphical illustrations.

A. MMSE-Power Charts

The optimal power allocation in (21), which is equivalent to (27), can be obtained by plotting $\gamma_i\texttt{MMSE}_i(p_i\gamma_i)$ as a function of $p_i \in [0, N]$ and finding its intercept with $\mu^* - \lambda^*\gamma_i$ for a given $\bar{Q}$. For instance, when $\bar{Q} = \bar{Q}_{ID}$ we have $\lambda^* = 0$ and the intercept of $\gamma_1\texttt{MMSE}_1(p_1\gamma_1)$ and $\gamma_2\texttt{MMSE}_2(p_2\gamma_2)$ with μ^* yields the optimal power allocations p_i^*. Fig. 2(a) illustrates this case in a SWIPT system having $N = 2$, $\gamma_1 = 4$, $\gamma_2 = 1.2$ and using a 4-QAM signal set. When $\bar{Q} > \bar{Q}_{ID}$, we have $\lambda^* > 0$ and the intercepting lines $\mu^* - \lambda^*\gamma_i$ differ for each of the channels depending on γ_i. Fig. 2(b)-(c) illustrate this case for three values of $\bar{Q} \in (\bar{Q}_{ID}, \bar{Q}_{max})$, which correspond to 10%, 50% and 90% of $\Delta\bar{Q} = \bar{Q}_{max} - \bar{Q}_{ID}$. It is evident from Fig. 2(d) that as $\bar{Q} \to \bar{Q}_{max}$, we arrive at $p_1^* \to N$, which is in accordance with Proposition 2.

Fig. 3 illustrates the optimal power allocation for various $\bar{Q}$ in the aforementioned SWIPT system for the 16-QAM case. The key difference between the 4-QAM and the 16-QAM case is that the stronger channel receives more power in the latter case, whereas in case of 4-QAM, the weaker channel may receive more power depending on the value of $\bar{Q}$. Note that the larger the size of the QAM constellation, closer it is to the Gaussian alphabet. Since a higher-gain channel receives more power in the Gaussian alphabet case, the power allocation in case of 16-QAM is quite similar. This phenomenon can be observed by comparing Fig. 2(a)-(b) to Fig. 3(a)-(b). Specifically, when $\bar{Q} = \bar{Q}_{ID}$, we have $p_2^* = 1.17$ and $p_1^* = 0.83$ in case of 4-QAM, whereas in case of 16-QAM we have $p_2^* = 0.8$ and $p_1^* = 1.2$. Note that in case of BPSK, this phenomenon occurs even for larger values of $\bar{Q}$. We have omitted the illustration of this scenario owing to the space constraint.

B. Mercury-Gallium Pouring

In this section, we provide an alternative interpretation of the mercury-gallium pouring algorithm, which is essentially a generalization of the mercury-water pouring algorithm presented in [19].

Let us define the following function, which measures the discrepancy w.r.t. the Gaussian input assumption:

$$G_i(\mu,\lambda) = \begin{cases} \frac{\gamma_i}{\mu-\lambda\gamma_i} - \texttt{MMSE}_i^{-1}\left(\frac{\mu-\lambda\gamma_i}{\gamma_i}\right), & \text{if } 0 \le \frac{\mu-\lambda\gamma_i}{\gamma_i} \le 1 \\ 1, & \text{otherwise.} \end{cases} \tag{33}$$

Note that the power allocation solution should satisfy

$$\frac{1}{\gamma_i}\left[\frac{\gamma_i}{\mu-\lambda\gamma_i} - \texttt{MMSE}_i^{-1}\left(\frac{\mu-\lambda\gamma_i}{\gamma_i}\right)\right] + p_i = \frac{1}{\mu-\lambda\gamma_i}.$$

When $G_i(\mu,\lambda) = 1$, we have $\frac{1}{\gamma_i} + p_i = \frac{1}{\mu-\lambda\gamma_i}$, which corresponds to the power allocation associated with the Gaussian input assumption. Thus, $G_i(\mu,\lambda)$ is a measure of discrepancy w.r.t. the Gaussian input assumption.

The power allocation solution presented in Proposition 4 can be interpreted as follows:

1) Set up a vessel having unit-base, which is solid up to the height $1/\gamma_i$ for the i^{th} channel.
2) For the specific μ and λ chosen, pour mercury up to the height $\frac{G_i(\mu,\lambda)}{\gamma_i}$ for the i^{th} channel.
3) Fill gallium up to the height $\frac{1}{\mu-\lambda\gamma_i}$ from the base for each of the i^{th} channel.

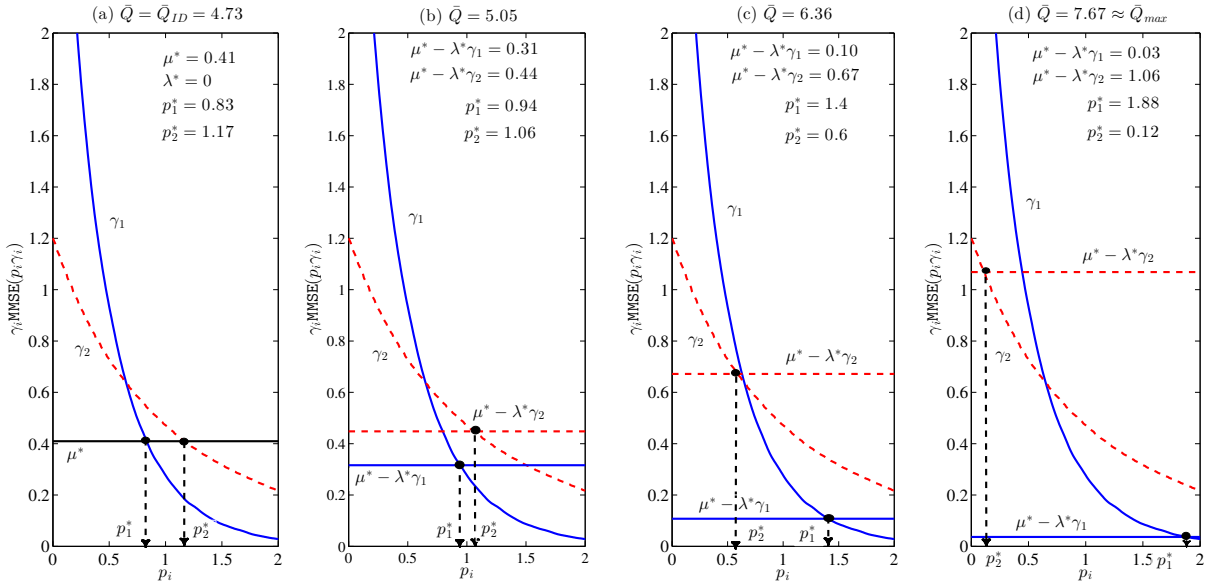

Fig. 2. The optimal power allocation for various $\bar{Q} \in (\bar{Q}_{ID}, \bar{Q}_{max})$ in a SWIPT system having $N = 2$, $\gamma_1 = 4$, $\gamma_2 = 1.2$ and employing 4-QAM.

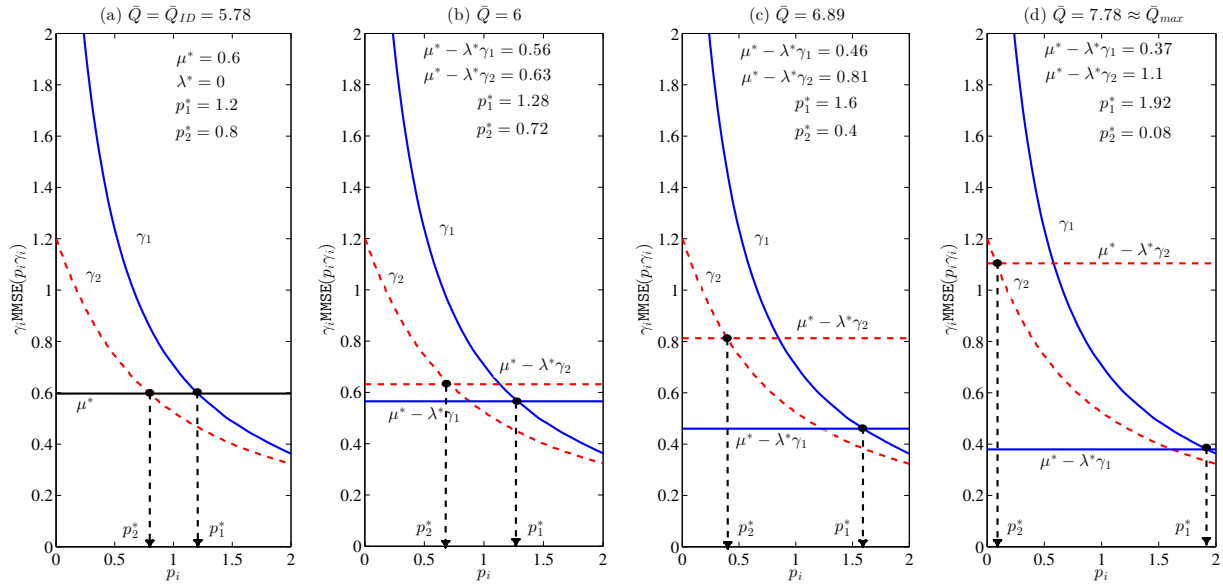

Fig. 3. The optimal power allocation for various $\bar{Q} \in (\bar{Q}_{ID}, \bar{Q}_{max})$ in a SWIPT system having $N = 2$, $\gamma_1 = 4$, $\gamma_2 = 1.2$ and employing 16-QAM.

4) The height of the gallium over the mercury in each of the vessels gives the optimal power allocation p_i^{MGP}.

Fig. 4(a) provides a pictorial depiction of the above interpretation of the mercury-gallium pouring algorithm. When $\lambda = 0$, which corresponds to the *no energy harvesting* constraint, the solution in (16) reduces to that of mercury-water pouring, as depicted in Fig. 4(b). It is readily seen that when $\lambda = 0$, the height $1/(\mu - \lambda\gamma_i) = 1/\mu$ up to which gallium has to be filled becomes fixed for all the channels.

V. Time Sharing and Power Splitting Schemes Operating with Finite Input Alphabet

In this section, we discuss practically feasible time sharing and power splitting aided SWIPT schemes operating with finite input alphabet and characterise their RE trade-off.

A. Time Sharing

Let us consider a SWIPT system in which the energy and the information transmission take place over independent time-slots. During the information transmission phase, only the ID

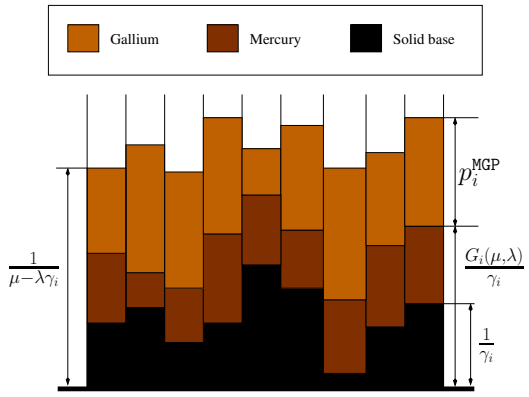

(a) Mercury–Gallium pouring

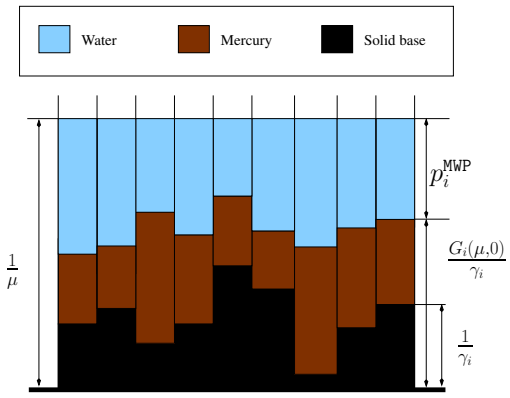

(b) Mercury–Water pouring

Fig. 4. Pictorial depiction of the mercury-gallium pouring solution presented in Proposition 4 and the mercury-water pouring algorithm proposed in [19].

receiver would be active, while in the energy transmission phase, only the EH receiver would be active. Let $0 \leq \alpha \leq 1$ denote the percentage of time allocated for EH. Let $\{p_i^{(1)}\}_{i=1}^N$ and $\{p_i^{(2)}\}_{i=1}^N$ represent the power allocations during the ID and EH phases, respectively. Under the fixed power constraint [7] for both EH and ID phases, we have

$$\mathcal{E}^{\mathtt{TS}_1}(P) \triangleq \bigcup_{\alpha\in[0,1]} \Big\{(R,\bar{Q}):\ R \leq (1-\alpha)\sum_{i=1}^{N}\mathcal{I}_i(p_i^{(1)}\gamma_i), \bar{Q} \leq \alpha\sum_{i=1}^{N} p_i^{(2)}\gamma_i, \sum_{i=1}^{N} p_i^{(j)} \leq N, j=1,2\Big\}, \tag{34}$$

where $\mathtt{TS}_1$ refers to the TS scheme having a fixed power constraint. The boundary of $\mathcal{E}^{\mathtt{TS}_1}(P)$ is essentially the line connecting the two extremities $(R_{max},0)$ and $(0,\bar{Q}_{max})$.

Under the flexible power constraint [7], where the transmission power averaged over the EH and ID phases is bounded, we have

$$\mathcal{E}^{\mathtt{TS}_2}(P) \triangleq \bigcup_{\alpha\in[0,1]} \Big\{(R,\bar{Q}):\ R \leq (1-\alpha)\sum_{i=1}^{N}\mathcal{I}_i(p_i^{(1)}\gamma_i), \bar{Q} \leq \alpha\sum_{i=1}^{N} p_i^{(2)}\gamma_i, (1-\alpha)\sum_{i=1}^{N} p_i^{(1)} + \alpha\sum_{i=1}^{N} p_i^{(2)} \leq N\Big\}, \tag{35}$$

where $\mathtt{TS}_2$ refers to the flexible power constraint. The following proposition provides a simplified RE region for the case of flexible power constraint, which is analogous to Proposition 4.1 of [7].

Proposition 6: Under the flexible power constraint, all the boundary points of $\mathcal{E}^{\mathtt{TS}_2}(P)$ except the two extremities $(R_{max},0)$ and $(0,\bar{Q}_{max})$ can be attained, when $\alpha \to 0$. Under this limiting condition, we have

$$\mathcal{E}^{\mathtt{TS}_2}(P) \triangleq \bigcup_{\alpha\in[0,1]} \Big\{(R,\bar{Q}): R \leq \sum_{i=1}^{N}\mathcal{I}_i(p_i^{(1)}\gamma_i), \sum_{i=1}^{N} p_i^{(1)} \leq N - \frac{\bar{Q}}{\gamma_1}, p_i^{(1)} \geq 0\ \forall i\Big\}. \tag{36}$$

The proof follows similar lines to that of Proposition 4.1 [7] and it is omitted due to space constraints. Note that for any $\bar{Q} < \bar{Q}_{max}$, the boundary point of $\mathcal{E}^{\mathtt{TS}_2}(P)$ in (36) is given by the mercury-water pouring algorithm described in Proposition 3. Furthermore, the limiting condition of $\alpha \to 0$ essentially assumes having infinite transmit power capability in the EH phase, which is practically infeasible. Under the finite transmit power condition, the optimal α that achieves the boundary points of $\mathcal{E}^{\mathtt{TS}_2}(P)$ can be shown to be $\alpha = \frac{\bar{Q}}{N\gamma_1 k_p}$, where $k_p = P_p/P$ and $P \leq P_p < \infty$ is the peak transmit power. Unless stated otherwise, $\mathtt{TS}_2$ refers to the time sharing scheme with $P_p = \infty$.

B. Power Splitting

Let us now consider a SWIPT system in which both the energy as well as the information transmission take place simultaneously. The receiver is assumed to have a power splitter that splits the received signal and simultaneously feeds both the EH as well as the ID receivers. Assuming uniform power splitting across all the N parallel channels, the achievable RE region is given by

$$\mathcal{E}^{\mathtt{UPS}}(P) \triangleq \bigcup_{\beta\in[0,1]} \Big\{(R,\bar{Q}):\ R \leq \sum_{i=1}^{N}\mathcal{I}_i(p_i\gamma_i(1-\beta)), \bar{Q} \leq \beta\sum_{i=1}^{N} p_i\gamma_i, \sum_{i=1}^{N} p_i \leq N\Big\}, \tag{37}$$

where β decides the fraction of the received power allocated for EH. The boundary points of the RE region given in (37) are obtained by the mercury-water pouring algorithm described in Proposition 3. A practical application of the above scheme arises, for instance, in the filter bank multi-carrier system [30], where each of the receive filters in the filterbank can be equipped with a power splitter that feeds both the EH and ID blocks.

C. High-SNR Asymptotics

A key requirement of the SWIPT systems is that they need a high SNR owing to the high energy threshold of the EH receiver. As a result, it is important to understand the behaviour of the various SWIPT schemes discussed earlier, when $P \to \infty$. Specifically, we study the asymptotic behaviour of $\texttt{TS}_2$ and $\texttt{UPS}$ schemes.

Proposition 7: When employing $\texttt{TS}_2$, the optimal power allocation under $P \to \infty$ is given by

$$p_i = \frac{N - \bar{q}}{|h_i|^2 \sum_{i=1}^{N} \frac{1}{|h_i|^2}}, \quad i = 1, \ldots, N, \tag{38}$$

where $\mathcal{S}_i$ is assumed to be the same for all the N parallel channels and $\bar{q} = \lim_{P\to\infty} \bar{Q}/\gamma_1$.

Proposition 8: When employing $\texttt{UPS}$, the optimal power allocation under $P \to \infty$ is given by

$$p_i = \frac{N}{|h_i|^2 \sum_{i=1}^{N} \frac{1}{|h_i|^2}}, \quad i = 1, \ldots, N, \tag{39}$$

where $\mathcal{S}_i$ is assumed to be the same for all the N parallel channels.

The proofs of both Proposition 7 and Proposition 8 follow from Theorem 5 [19] and are omitted due to space constraints. Note that the asymptotic power allocation in (38) depends on the harvested energy through $\bar{q}$, whereas that in (39) does not depend on the harvested energy. Furthermore, the power allocation in (39) is the same as that of the system operating without energy harvesting [19]. Considering the low-complexity nature of $\texttt{TS}_2$ and its explicit dependence on $\bar{Q}$, we restrict our attention to $\texttt{TS}_2$ while evaluating the asymptotic high-SNR performance.

D. Performance Evaluation

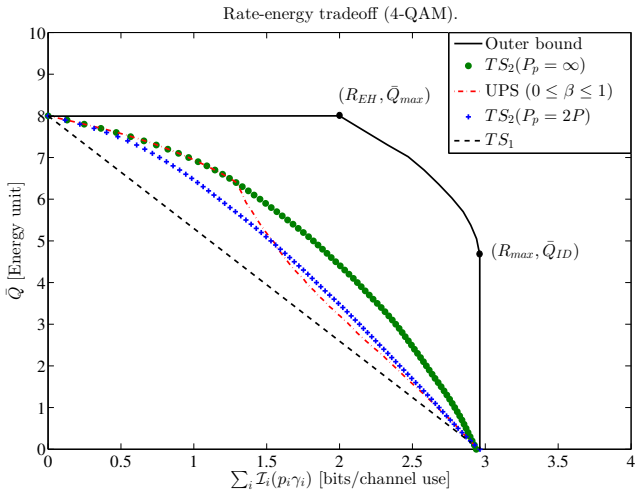

Fig. 5. Comparison of the achievable RE trade-off by various schemes in a SWIPT system having $N = 2$, $\gamma_1 = 4$, $\gamma_2 = 1.2$ and employing 4-QAM signal set over both the channels.

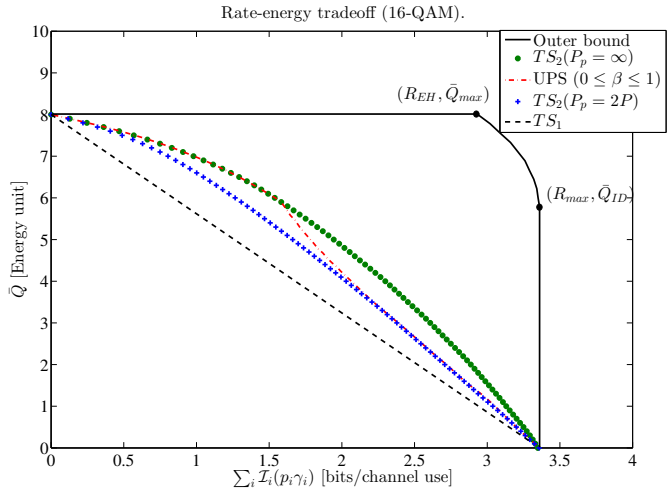

Fig. 6. The achievable RE trade-off by various schemes when employing 16-QAM signal set over both the channels. The system parameters are same as that of Fig. 5.

1) RE Tradeoff: Let us now compare the RE trade-off attained by the various schemes discussed so far. Consider a SWIPT system having $N = 2$, $\gamma_1 = 4$ and $\gamma_2 = 1.2$. Fig. 5 compares the RE trade-off using the 4-QAM signal set over both the channels. The outer bound along with the RE regions of $\texttt{TS}_1$, and of $\texttt{TS}_2$ using $P_p = 2P$ as well as $P_p = \infty$ transmit peak power constraints and that of the $\texttt{UPS}$ scheme are depicted in Fig. 5. It can be seen from Fig. 5 that $\mathcal{E}^{\texttt{TS}_1}(P) \subseteq \mathcal{E}^{\texttt{TS}_2}(P)$. The RE region of $\texttt{TS}_2$ with finite P_p as well as that of $\texttt{UPS}$ are observed to lie between $\mathcal{E}^{\texttt{TS}_1}(P)$ and $\mathcal{E}^{\texttt{TS}_2}(P)$, as in the Gaussian alphabet case [7]. In case of UPS, when β is large, a large fraction of the received power is allocated to energy harvesting. As a result, a small fraction of power is available for information transmission. In this case, only the channel having the highest gain receives all the available power. When β is decreased, more power becomes available for information transmission, hence multiple channels may receive non-zero power allocation. This is evident from Fig. 5, where the trade-off curve associated with the UPS shows two different trends. Fig. 6 compares the RE trade-off in the aforementioned system for the 16-QAM signal set. Note that all the observations made from Fig. 5 hold for this case as well. Thus, we can conclude from Fig. 5 and Fig. 6 that the relative performance trends of the various schemes under finite input alphabet are similar to those of Gaussian input alphabet (cf. Section IV-D [7]).

2) Optimal vs. Asymptotic Power Allocation: Let us compare the performance of the asymptotic power allocation of (38) to that of the optimal power allocation discussed in Section V-A. Fig. 7 compares the attainable RE trade-off when employing both optimal and asymptotic power allocations for various values of P. The system is assumed to have $N = 2$, $|h_1|^2 = 4$, $|h_2|^2 = 1.2$ and using the 2-PAM signal set over both the channels. It is evident from Fig. 7 that when $\bar{Q}$ is negligible, the asymptotic and optimal power allocations attain nearly the same performance. Furthermore, when the operating rate is much lower than R_{max}, we see that both

the asymptotic and optimal power allocations give nearly the same performance. Since most of the practical systems employ channel codes whose rates are much less than one, the asymptotic power allocation would be a suitable low-complexity solution.

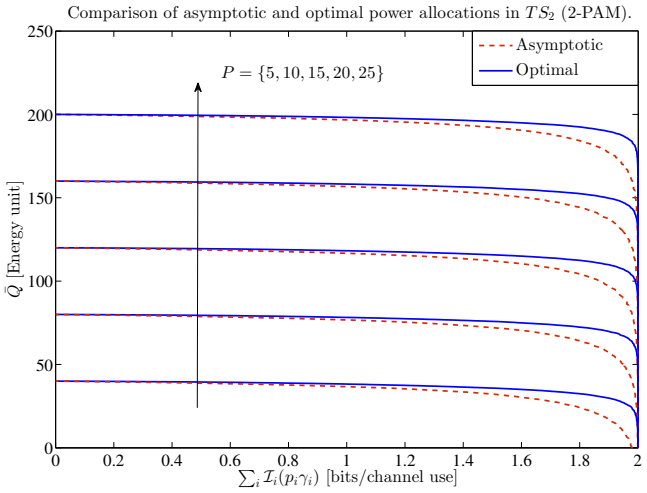

Fig. 7. Comparison of the achievable RE trade-off in a SWIPT system employing $\texttt{TS}_2$ with optimal and asymptotic power allocations. The system parameters are assumed to be $N = 2$, $|h_1|^2 = 4$, $|h_2|^2 = 1.2$ and 2-PAM signal set over both the channels.

Fig. 8 and Fig. 9 compare the attained RE trade-off by optimal and asymptotic power allocations in case of the 4-QAM and 16-QAM signal sets, respectively. It is evident from Fig. 7, Fig. 8 and Fig. 9 that the performance loss with respect to the optimal power allocation increases, when the size of the signal set is increased. However, when the operating datarate is lower than R_{max}, we can still employ the asymptotic power allocation without incurring a significant performance loss.

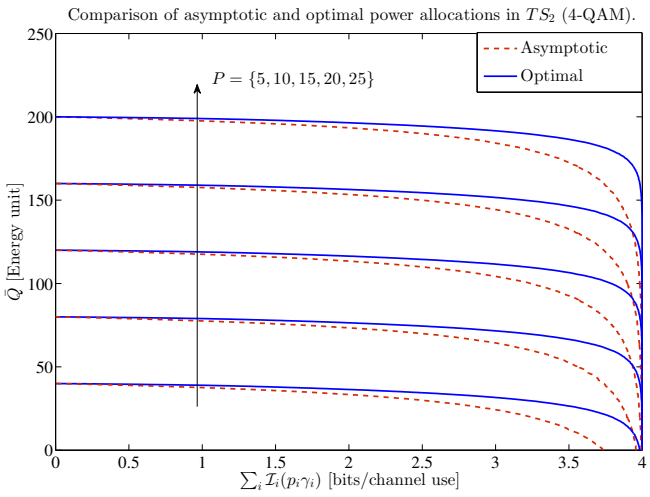

Fig. 8. Comparison of the achievable RE trade-off when operating with 4-QAM signal set over both the channels. The system parameters are same as that of Fig. 7.

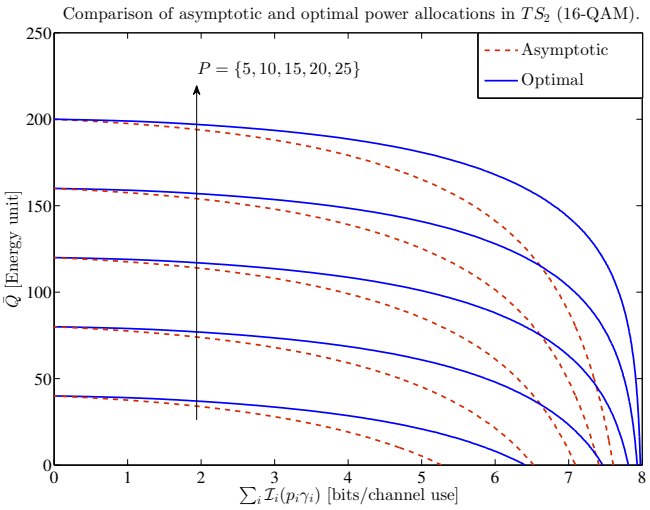

Fig. 9. Comparison of the achievable RE trade-off when operating with 16-QAM signal set over both the channels. The system parameters are same as that of Fig. 7.

3) Optimal vs. Gaussian Power Allocation [7]: A key difference in the performance of the Gaussian and finite input alphabets such as QAM/PSK is that in the latter case the associated MI saturates with the SNR, hence resulting in no further incentive for any additional power allocation, which is in contrast to the Gaussian alphabet case, where the associated MI does not saturate with the SNR. This key difference renders the SWIPT schemes that assume Gaussian input alphabets suboptimal for practical systems, which employ practical QAM/PSK constellations. We quantify the penalty of the Gaussian input assumption both in terms of the attainable MI as well as the harvested energy, and show that the penalty imposed by this assumption can be severe, when the modulation alphabet is small. In the following, the Gaussian power allocation refers to the power allocation policy assuming Gaussian input alphabet [7].

Fig. 10 compares the RE trade-off in a SWIPT system employing $\texttt{TS}_2$ using both optimal as well as Gaussian power allocations. The signal sets considered are 2-PAM, 4-QAM and 16-QAM, and the transmission powers considered are given by $P \in \{5, 15, 25\}$. The system is assumed to have $N = 2$ and the channel powers are assumed to be $|h_1|^2 = 4$ and $|h_2|^2 = 1.2$, as earlier. It is evident from Fig. 10 that the Gaussian power allocation is outperformed by the optimal power allocation for all the signal sets considered, especially in the Pareto frontier region. Table I quantifies the rate-penalty imposed by the Gaussian power allocation.

So far, we studied the performance of both the Gaussian and optimal power allocations by considering fixed channel gains. Let us now compare their performance as a function of the channel powers. This is accomplished in Fig. 11 by studying the achievable rate as a function of $\frac{\gamma_2}{\gamma_1}$ between -20 dB to 0 dB. The signal set employed over both the channels is 2-PAM and the transmit power is $P = 25$. It is evident from Fig. 11 that as the difference between γ_2 and γ_1 increases, the rate-penalty of the Gaussian power allocation becomes more

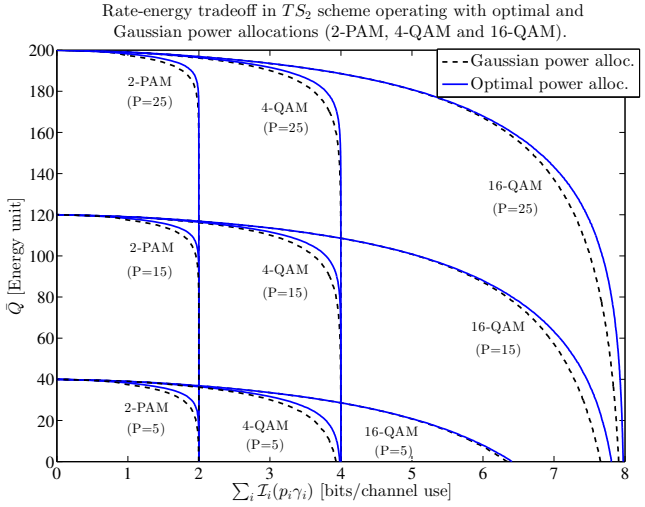

Fig. 10. Comparison of the RE trade-off in a SWIPT system employing $\mathtt{TS}_2$ with optimal and Gaussian power allocations for various signal sets and transmission powers. The system parameters are assumed to be $N = 2$, $|h_1|^2 = 4$ and $|h_2|^2 = 1.2$.

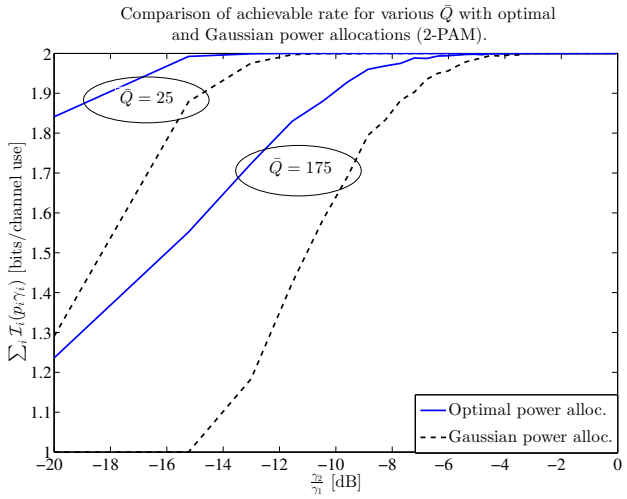

Fig. 11. Comparison of the achievable rate as a function of $\left(\frac{\gamma_2}{\gamma_1}\right)$ in a SWIPT system employing $\mathtt{TS}_2$ with optimal and Gaussian power allocations. The system is assumed to operate with 2-PAM signal set over both the channels.

TABLE I
COMPARISON OF THE ACHIEVABLE RATE BY GAUSSIAN AND OPTIMAL POWER ALLOCATIONS WHEN $P = 25$.

Signal set	Rate attained by Gaussian power allocation.	Rate attained by optimal power allocation.
2-PAM ($\bar{Q} = 195$)	1.40	1.59
4-QAM ($\bar{Q} = 182$)	3.54	3.72
16-QAM ($\bar{Q} = 100$)	7.50	7.68

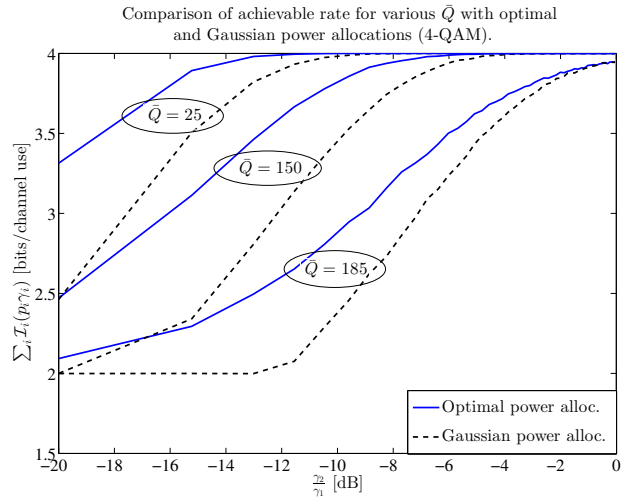

Fig. 12. The performance of the system considered in Fig. 10 when operating with 4-QAM signal set over both the channels.

pronounced. When $\bar{Q} = 175$ and $\frac{\gamma_2}{\gamma_1} < -15$ dB, we observe that the Gaussian power allocation does not allocate any power to the 2nd channel, hence the achievable rate saturates at 1 bits/channel use. By contrast, the optimal power allocation ensures that the weaker channel gleans sufficient power, while the stronger channel does not receive more power than what is optimal for the 2-PAM signal set. Similar observations hold for the 4-QAM case depicted in Fig. 12. It is evident from Fig. 12 that as $\bar{Q}$ increases, the achievable rate becomes more sensitive to $\frac{\gamma_2}{\gamma_1}$. This is indeed expected, since the power available for information transmission reduces when $\bar{Q}$ increases, where the specific power allocation policy employed plays an influential role. Table II quantifies the rate-penalty of the Gaussian power allocation for the 4-QAM signal set. It is evident from Table II that when $\bar{Q}$ is sufficiently large, the optimal power allocation significantly outperforms the Gaussian power allocation. Specifically, a rate improvement of about 20% and 30% is observed for $\bar{Q} = 150$ and $\bar{Q} = 185$, respectively.

Let us now study the RE trade-off attainable over the fading channel. Since the attainable rate as well as the harvested energy differ for each channel realization, we consider ergodic rate and the normalized harvested energy denoted by $\bar{Q}_n = \frac{\bar{Q}}{\gamma_1}$ $(0 \leq \bar{Q}_n \leq N)$ for characterising the RE trade-off. Consider a 2×2 MIMO system employing SVD aided beamforming and 4-QAM signal set over both the channels. Fig. 13 compares the attainable RE trade-off in the aforementioned system when employing Gaussian and optimal power allocations for $P = 5$ and $P = 15$. It is evident from Fig. 13 that the the optimal power allocation significantly outperforms the Gaussian power allocation. Specifically, when $\bar{Q}_n = 1$ a rate improvements of 0.3 and 0.35 bits/channel use are observed when $P = 5$ and $P = 15$, respectively.

Fig. 14 compares the attainable RE trade-off in a 3×3 MIMO system employing SVD aided beamforming and 2-PAM signal set over all the channels. It is evident from Fig. 14 that the Gaussian power allocation suffers from performance loss compared to the optimal power allocation as in the 4-QAM case (cf. Fig. 13). Specifically, the optimal power

TABLE II
COMPARISON OF THE ACHIEVABLE RATE BY GAUSSIAN AND OPTIMAL POWER ALLOCATIONS IN CASE OF 4-QAM WHEN $\frac{\gamma_2}{\gamma_1} = -12\ dB$.

$\bar{Q}$	Rate attained by Gaussian power allocation.	Rate attained by optimal power allocation.
25	3.90	3.98
150	3.03	3.60
185	2.05	2.60

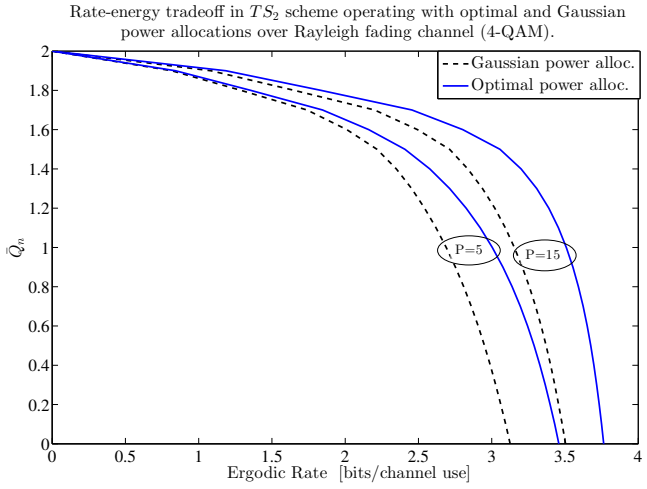

Fig. 13. Comparison of the achievable RE trade-off in a SWIPT system employing $\texttt{TS}_2$ and operating over 2×2 Rayleigh fading channel with the aid of beamforming. The system is assumed to operate with 4-QAM signal set over both the channels.

allocation attains a power gain of about 26% when operating at 2.75 bits/channel use and $P = 5$, and about 40% when operating at 2.9 bits/channel use and $P = 15$, respectively.

E. Future Directions

In this paper, we have studied the performance of SWIPT systems considering realistic signal constellations such as BPSK/QAM. These classic signal sets are known to be less energy-efficient than multi-dimensional signal sets such as spatial modulation (SM) [31], [32]. The SM is capable of striking more beneficial design trade-offs owing to using a low number of RF chains and low-complexity maximum likelihood decoding complexity [33]. It would be interesting to study the RE trade-off in SWIPT systems employing SM. Furthermore, the existing literature mainly focuses on SWIPT in multicarrier systems [9], [34]. However, multicarrier systems tend to require complex power-hungry signal processing and hence they are less suitable for battery-operated devices. By contrast, single carrier transmission schemes [35] are a suitable choice. It would be interesting to study the attainable RE trade-off in single carrier schemes employing SM and classic signal sets, which has hitherto not been studied. There has been a significant interest in SWIPT-enabled full-duplex systems [36],

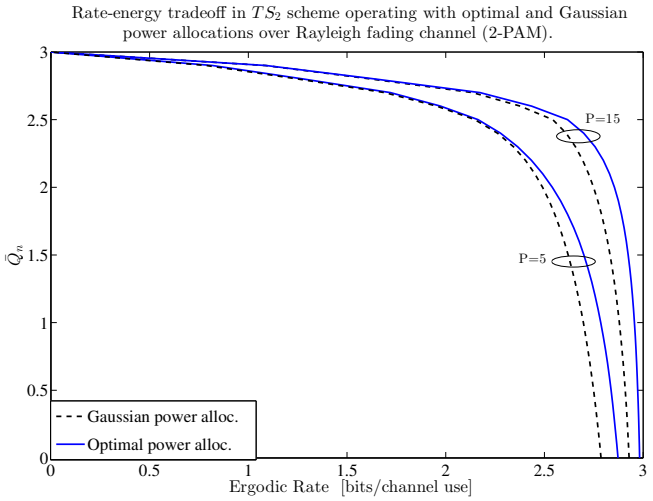

Fig. 14. Comparison of the achievable RE trade-off in a SWIPT system employing $\texttt{TS}_2$ and operating over 3×3 Rayleigh fading channel with the aid of beamforming. The system is assumed to operate with 2-PAM signal set over all the channels.

[37]. It would be worthwhile studying the attainable RE trade-off in these systems considering finite input alphabets.

VI. CONCLUSIONS

We have characterised the RE trade-off in SWIPT systems operating with finite input alphabet over parallel Gaussian channels, which has hitherto not been studied in the literature. The RE trade-off of the SWIPT system operating with Gaussian input alphabet was shown to be a special case of our result (cf. Corollary 1). The Gaussian input assumption was observed to significantly overestimate the actual attainable RE trade-off with finite input alphabets. Further insights into our results were provided with the aid of graphical illustrations: a) MMSE-power charts and b) Mercury-Gallium pouring algorithm. Furthermore, the proposed mercury-gallium pouring algorithm was shown to be a generalization of the well-known mercury-water pouring algorithm. Practically relevant time sharing and power splitting schemes were discussed and their RE trade-off was characterised considering finite input alphabet. Furthermore, their asymptotic power allocation solutions were obtained, which were shown to be optimal except for the Pareto frontier region. Furthermore, the attainable RE trade-off with Gaussian and finite input alphabet were studied by considering various signal sets and transmit powers. The rate attained by the optimal power allocation was observed to be significantly better than that of Gaussian power allocation.

REFERENCES

[1] T. Taleb and A. Kunz, "Machine type communications in 3GPP networks: potential, challenges, and solutions," *IEEE Commun. Mag.*, vol. 50, no. 3, pp. 178-184, Mar. 2012.

[2] S. Bi, C. K. Ho and R. Zhang, "Wireless powered communication: opportunities and challenges," *IEEE Commun. Mag.*, vol. 53, no. 4, pp. 117-125, Apr. 2015.

[3] X. Chen, Z. Zhang, H. H. Chen and H. Zhang, "Enhancing wireless information and power transfer by exploiting multi-antenna techniques," *IEEE Commun. Mag.*, vol. 53, no. 4, pp. 133-141, Apr. 2015.

[4] Z. Ding *et al.*, "Application of smart antenna technologies in simultaneous wireless information and power transfer," *IEEE Commun. Mag.*, vol. 53, no. 4, pp. 86-93, Apr. 2015.

[5] L. R. Varshney, "Transporting information and energy simultaneously," *in Proc. 2008 IEEE International Symposium on Information Theory, Toronto, ON*, pp. 1612-1616, Aug. 2008.

[6] P. Grover and A. Sahai, "Shannon meets Tesla: Wireless information and power transfer," *in Proc. 2010 IEEE International Symposium on Information Theory, Austin, TX*, pp. 2363-2367, July 2010.

[7] R. Zhang and C. K. Ho, "MIMO broadcasting for simultaneous wireless information and power transfer," *IEEE Trans. Wireless Commun.*, vol. 12, no. 5, pp. 1989-2001, May 2013.

[8] X. Zhou, R. Zhang and C. K. Ho, "Wireless information and power transfer: architecture design and rate-energy trade-off," *IEEE Trans. Commun.*, vol. 61, no. 11, pp. 4754-4767, Nov. 2013.

[9] X. Zhou, R. Zhang and C. K. Ho, "Wireless information and power transfer in multiuser OFDM systems," *IEEE Trans. Wireless Commun.*, vol. 13, no. 4, pp. 2282-2294, Apr. 2014.

[10] Y. Zeng, B. Clerckx and R. Zhang, "Communications and signals design for wireless power transmission," *IEEE Trans. Commun.*, vol. 65, no. 5, pp. 2264-2290, May 2017.

[11] B. Clerckx, "Wireless information and power transfer: nonlinearity, waveform design, and rate-energy trade-off," *IEEE Trans. Signal Process.*, vol. 66, no. 4, pp. 847-862, Feb. 2018.

[12] X. Chen, C. Yuen and Z. Zhang, "Wireless energy and information transfer trade-off for limited-feedback multiantenna systems with energy beamforming," *IEEE Trans. Veh. Technol.*, vol. 63, no. 1, pp. 407-412, Jan. 2014.

[13] Q. Shi, L. Liu, W. Xu and R. Zhang, "Joint transmit beamforming and receive power splitting for MISO SWIPT systems," *IEEE Trans. Wireless Commun.*, vol. 13, no. 6, pp. 3269-3280, June 2014.

[14] J. Park and B. Clerckx, "Joint wireless information and energy transfer with reduced feedback in MIMO interference channels," *IEEE J. Sel. Areas Commun.*, vol. 33, no. 8, pp. 1563-1577, Aug. 2015.

[15] O. T. Demir and T. E. Tuncer, "Antenna selection and hybrid beamforming for simultaneous wireless information and power transfer in multi-group multicasting systems," *IEEE Trans. Wireless Commun.*, vol. 15, no. 10, pp. 6948-6962, Oct. 2016.

[16] L. Yang, Y. Zeng and R. Zhang, "In-band wireless information and power transfer with lens antenna array," *IEEE Commun. Lett.*, vol. 21, no. 1, pp. 100-103, Jan. 2017.

[17] D. Guo, S. Shamai and S. Verdu, "Mutual information and minimum mean-square error in Gaussian channels," *IEEE Trans. Inf. Theory*, vol. 51, no. 4, pp. 1261-1282, Apr. 2005.

[18] D. P. Palomar and S. Verdu, "Gradient of mutual information in linear vector Gaussian channels," *IEEE Trans. Inf. Theory*, vol. 52, no. 1, pp. 141-154, Jan. 2006.

[19] A. Lozano, A. M. Tulino and S. Verdu, "Optimum power allocation for parallel Gaussian channels with arbitrary input distributions," *IEEE Trans. Inf. Theory*, vol. 52, no. 7, pp. 3033-3051, July 2006.

[20] C. Xiao, Y. R. Zheng and Z. Ding, "Globally optimal linear precoders for finite alphabet signals over complex vector Gaussian channels," *IEEE Trans. Signal Process.*, vol. 59, no. 7, pp. 3301-3314, July 2011.

[21] W. Zeng, C. Xiao, J. Lu, and K. B. Letaief, "Globally optimal precoder design with finite-alphabet inputs for cognitive radio networks," *IEEE J. Sel. Areas Commun.*, vol. 30, no. 10, pp. 1861-1873, Nov. 2012.

[22] R. Rajashekar and L. Hanzo, "Hybrid beamforming in mm-Wave MIMO systems having a finite input alphabet," *IEEE Trans. Commun.*, vol. 64, no. 8, pp. 3337-3349, Aug. 2016.

[23] Y. Wu, D. W. K. Ng, C. K. Wen, R. Schober and A. Lozano, "Low-complexity MIMO precoding for finite-alphabet signals," *IEEE Trans. Wireless Commun.*, vol. 16, no. 7, pp. 4571-4584, July 2017.

[24] T. A. Zewde and M. C. Gursoy, "Simultaneous wireless information and power transfer with finite-alphabet input signals," *in proc. 2015 IEEE 82nd Vehicular Technology Conference (VTC2015-Fall), Boston, MA*, pp. 1-5, Jan. 2016.

[25] X. Zhu, W. Zeng and C. Xiao, "Precoder design for simultaneous wireless information and power transfer with finite-alphabet inputs," *in Proc. 2017 IEEE Wireless Communications and Networking Conference (WCNC), San Francisco, CA*, pp. 1-5, May 2017.

[26] X. Zhu, W. Zeng and C. Xiao, "Precoder design for simultaneous wireless information and power transfer systems with finite-alphabet inputs," *IEEE Trans. Veh. Technol.*, vol. 66, no. 10, pp. 9085-9097, Oct. 2017.

[27] J. A. C. Bingham, "Multicarrier modulation for data transmission: An idea whose time has come," *IEEE Commun. Mag.*, vol. 28, no. 5, pp. 5-14, May 1990.

[28] D. Tse and P. Viswanath, "Fundamentals of wireless communication." *Cambridge University Press*, 2005.

[29] S. Boyd and L. Vandenberghe, "Convex optimization." *Cambridge, U.K.: Cambridge Univ. Press*, 2004.

[30] B. Farhang-Boroujeny, "OFDM versus filter bank multicarrier," *IEEE Signal Process. Mag.*, vol. 28, no. 3, pp. 92-112, May 2011.

[31] R. Mesleh, H. Haas, S. Sinanovic, C. Ahn and S. Yun "Spatial modulation," *IEEE Trans. Veh. Technol.*, vol. 57, no. 4, pp. 2228-2242, July 2008.

[32] A. Stavridis, S. Sinanovic, M. Di Renzo and H. Haas, "Energy evaluation of spatial modulation at a multi-antenna base station," *in Proc. 2013 IEEE 78th Vehicular Technology Conference (VTC Fall)*, Las Vegas, NV, Sep. 2013.

[33] R. Rajashekar, K.V.S. Hari, L. Hanzo, "Reduced-complexity ML detection and capacity-optimized training for spatial modulation systems," *IEEE Trans. Commun.*, vol. 62, no. 1, pp. 112-125, Jan. 2014.

[34] K. Huang and E. Larsson, "Simultaneous information and power transfer for broadband wireless systems," *IEEE Trans. Signal Process.*, vol. 61, no. 23, pp. 5972-5986, Dec. 2013.

[35] R. Rajashekar, K.V.S. Hari and L. Hanzo, "Spatial modulation aided zero-padded single carrier transmission for dispersive channels," *IEEE Trans. Commun.*, vol. 61, no. 6, pp. 2318-2329, June 2013.

[36] C. Zhong, H. A. Suraweera, G. Zheng, I. Krikidis and Z. Zhang, "Wireless information and power transfer with full duplex relaying," *IEEE Trans. Commun.*, vol. 62, no. 10, pp. 3447-3461, Oct. 2014.

[37] Y. Zeng and R. Zhang, "Full-duplex wireless-powered relay with self-energy recycling," *IEEE Wireless Commun. Lett.*, vol. 4, no. 2, pp. 201-204, Apr. 2015.

Rakshith Rajashekar (M'14-SM'17) received the B.E. degree in electrical communication engineering from Visvesvaraya Technological University, Karnataka, India, in 2007. He received his Ph.D. from the Department of Electrical Communication Engineering, Indian Institute of Science (IISc), India, in 2014. He is presently working as a Research Fellow at the University of Southampton, UK. Before joining the University of Southampton, he worked at Accord Software & Systems, Bengaluru, India, as a Systems Engineer from 2007 to 2009, and as a Senior Scientist at Broadcom Communications, Bengaluru, India from 2014 to 2015. His research interests include antenna selection in MIMO systems, differential communication, millimeter wave communication, communication between drones with a focus on space-time signal processing and coding. He is the recipient of the Special Recognition award from Broadcom Communications, India and the Dean's Award from the University of Southampton, UK, for excellence in research. He has received the Best Reviewer award from IEEE Transactions on Wireless Communications, IEEE Transactions on Communications and IEEE Wireless Communications Letters.

Marco Di Renzo (S'05-AM'07-M'09-SM'14) was born in L'Aquila, Italy, in 1978. He received the Laurea (cum laude) and the Ph.D. degrees in electrical engineering from the University of L'Aquila, Italy, in 2003 and in 2007, respectively, and the Doctor of Science degree (HDR) from University Paris-Sud, France, in 2013. Since 2010, he has been a CNRS Associate Professor ("Chargé de Recherche Titulaire CNRS") in the Laboratory of Signals and Systems of Paris-Saclay University – CNRS, CentraleSupélec, Univ Paris Sud, Paris, France. He is an Adjunct Professor at the University of Technology Sydney, Australia, a Visiting Professor at the University of L'Aquila, Italy, and a Co-Founder of the university spin-off company WEST Aquila s.r.l., Italy. He serves as the Associate Editor-in-Chief of IEEE COMMUNICATIONS LETTERS, and as an Editor of IEEE TRANSACTIONS ON COMMUNICATIONS, and IEEE TRANSACTIONS ON WIRELESS COMMUNICATIONS. He is a Distinguished Lecturer of the IEEE Vehicular Technology Society and IEEE Communications Society. He is the Project Coordinator of the European-funded projects H2020-MSCA ETN-5Gwireless and H2020-MSCA ETN-5Gaura. He is a recipient of several awards, including the 2013 IEEE-COMSOC Best Young Researcher Award for Europe, Middle East and Africa (EMEA Region), the 2013 NoE-NEWCOM# Best Paper Award, the 2014-2015 Royal Academy of Engineering Distinguished Visiting Fellowship, the 2015 IEEE Jack Neubauer Memorial Best System Paper Award, the 2015-2018 CNRS Award for Excellence in Research and in Advising Doctoral Students, the 2016 MSCA Global Fellowship (declined), the 2017 SEE-IEEE Alain Glavieux Award, the 2018 IEEE ICNC Silver Contribution Award, and 6 Best Paper Awards at IEEE conferences (2012 and 2014 IEEE CAMAD, 2013 IEEE VTC-Fall, 2014 IEEE ATC, 2015 IEEE ComManTel, 2017 IEEE SigTelCom).

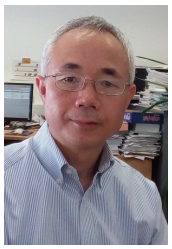

Lie-Liang Yang (M'98, SM'02, F'16) received his BEng degree in communications engineering from Shanghai TieDao University, Shanghai, China in 1988, and his MEng and PhD degrees in communications and electronics from Northern (Beijing) Jiaotong University, Beijing, China in 1991 and 1997, respectively. From June 1997 to December 1997 he was a visiting scientist of the Institute of Radio Engineering and Electronics, Academy of Sciences of the Czech Republic. Since December 1997, he has been with the University of Southampton, United Kingdom, where he is the professor of wireless communications in the School of Electronics and Computer Science. He has research interest in wireless communications, wireless networks and signal processing for wireless communications, as well as molecular communications and nano-networks. He has published over 360 research papers in journals and conference proceedings, authored/co-authored three books and also published several book chapters. The details about his research publications can be found at http://www.mobile.ecs.soton.ac.uk/lly/. He is a fellow of both the IEEE and the IET, and a distinguished lecturer of the IEEE. He served as an associate editor to the IEEE Trans. on Vehicular Technology and Journal of Communications and Networks (JCN), and is currently an associate editor to the IEEE Access and the Security and Communication Networks (SCN) Journal.

K.V.S. Hari (M'92-SM'97-F'15) received the B.E. degree from Osmania University, Hyderabad, India, in 1983; the M.Tech. degree from the Indian Institute of Technology Delhi, New Delhi, India, in 1985; and the Ph.D. degree from the University of California at San Diego, La Jolla, CA, USA, in 1990.Since 1992, he has been with the Department of Electrical Communication Engineering, Indian Institute of Science, Bangalore, India, where he is currently a Professor and coordinates the activities of the Statistical Signal Processing Laboratory. His research interests include the development of signal processing algorithms for MIMO wireless communication systems, sparse signal recovery problems, indoor positioning, assistive technologies for the elderly, and neuroscience. He was an Affiliated Professor (2010-16) with the Department of Signal Processing, KTH Royal Institute of Technology, Stockholm, Sweden. He has been a Visiting Faculty Member with Stanford University, Stanford, CA, USA; KTH Royal Institute of Technology, Stockholm, Sweden; and Aalto University, Espoo, Finland (formerly Helsinki University of Technology). While at Stanford University, he worked on multiple-input multiple-output (MIMO) wireless channel modelling and co-authored the Worldwide Interoperability for Microwave Access standard on wireless channel models for fixed-broadband wireless communication systems, which proposed the Stanford University Interim channel models. He was also with the Defence Electronics Research Laboratory, Hyderabad, and the Research and Training Unit for Navigational Electronics, Osmania University. Dr. Hari was an Editor of Elsevier's EURASIP journal Signal Processing (2006- 16) and the Senior Associate Editor (2013-18) and currently the Editor (Electrical Sciences) of Springer's Indian Academy of Sciences journal, SADHANA. He is an Academic Entrepreneur and a Cofounder of the company ESQUBE Communication Solutions, Bangalore. He received the Institution of Electronics and Telecommunication Engineers S. V. C. Aiya Award for Excellence in Telecom Education and the Distinguished Alumnus Award from the Osmania University College of Engineering, Hyderabad. He is a Fellow of the Indian National Academy of Engineering.

Lajos Hanzo (http://www-mobile.ecs.soton.ac.uk) FREng, FIEEE, FIET, Fellow of EURASIP, DSc received his degree in electronics in 1976 and his doctorate in 1983. In 2009 he was awarded an honorary doctorate by the Technical University of Budapest and in 2015 by the University of Edinburgh. In 2009 he was awarded an honorary doctorate by the Technical University of Budapest and in 2015 by the University of Edinburgh. In 2016 he was admitted to the Hungarian Academy of Science. During his 40-year career in telecommunications he has held various research and academic posts in Hungary, Germany and the UK. Since 1986 he has been with the School of Electronics and Computer Science, University of Southampton, UK, where he holds the chair in telecommunications. He has successfully supervised 112 PhD students, co-authored 18 John Wiley/IEEE Press books on mobile radio communications totalling in excess of 10 000 pages, published 1771 research contributions at IEEE Xplore, acted both as TPC and General Chair of IEEE conferences, presented keynote lectures and has been awarded a number of distinctions. Currently he is directing a 60-strong academic research team, working on a range of research projects in the field of wireless multimedia communications sponsored by industry, the Engineering and Physical Sciences Research Council (EPSRC) UK, the European Research Council's Advanced Fellow Grant and the Royal Society's Wolfson Research Merit Award. He is an enthusiastic supporter of industrial and academic liaison and he offers a range of industrial courses. He is also a Governor of the IEEE ComSoc and VTS. During 2008 - 2012 he was the Editor-in-Chief of the IEEE Press and a Chaired Professor also at Tsinghua University, Beijing. For further information on research in progress and associated publications please refer to http://www-mobile.ecs.soton.ac.uk